Self-Rolling of Oxide Nanomembranes and Resonance Coupling in Tubular Optical Microcavity

*Xianyun Lin, Yangfu Fang, Lingjia Zhu, Jing Zhang, Gaoshan Huang, Jiao Wang, and Yongfeng Mei**

Nanomembrane self-rolling offers the manufacture flexibility of 3D architectures for various applications in photonics, robotics, electronics, etc. Rolled-up oxide microtubes fabricated by both wet chemical etching and dry-releasing methods enable a broad range tuning of diameters (from 1 to 15 μm) and therefore same to their optical whispering gallery modes (WGMs). Their thin walls (several tens of nanometers) of such tubular optical microcavities provide strongly on-resonance coupling of attached dye emitters to optical modes, which leads to a cavity enhancement for Raman scattering without importing noble metal. Rolled-up thin-walled oxide tubular microcavity delivers a new optical component for light coupling and may imply interesting applications in the interaction between light and matter.

1. Introduction

Optical whispering gallery modes (WGMs)[1,2] microcavities have attracted considerable research attention due to their extensive potential applications in, e.g., photonics and integrated optics.[3,4] Tubular optical microcavity with WGMs offers unique capability of on-chip integration[5–7] and fluidic handling for analysis[8–11] besides excellent characteristic of optical microcavity.[12,13] Rolled-up nanotechnology employs a conventional top-down approach together with a self-rolling process and constructs prestressed nanomembranes with arbitrary shapes and various materials into a tubular geometry upon strain releasing.[1,2,5–7,10] Since the wall of rolled-up tubular optical cavities is thinner than the light resonance wavelength, its evanescent field can ensure an efficient coupling between the external emitters[14] or analytes[8,9,11] and the resonant modes, which suggests application potential in liquid refractometers for bioanalytical systems[15] or optofluidic microlasers.[16] The field distribution along the radial direction of microtubes reveals the evanescent regime outside of the tube wall and the nonevanescent regime inside the wall.[17,18] The coupling of external objects into the evanescent regime outside of optical microcavity can lead to interesting properties or applications like single nanoparticle detection[19] or strong nitrogen vacancy (NV) centers emission in diamond.[20] Furthermore, a strong coupling of absorbed light-active materials in the nonevanescent regime can deliver improved surface or absorption sensing performance.[17,21] Here, we demonstrate that dye molecules are well absorbed in the oxide tube walls (the nonevanescent regime) for enhanced coupling effect, e.g., photoluminescence and Raman scattering. Such oxide microtubes are self-rolled-up from oxide nanomembranes with various materials under wet chemical or dry etching methods for a broad range tuning of diameters ranging from submicrometer and several tens of micrometers, where the microtubes with small diameters support WGM resonance as those with big diameters. The dye molecules (Rhodamine 6G, R6G) introduced into the microtube wall are coupled into WGM resonance, which are characterized by means of microphotoluminescence (μ-PL) and Raman measurements. Such dye-decorated hybrid system may enable tubular optical microcavities as a new type platform for optofluidic sensing and lasing.

X. Y. Lin, Y. F. Fang, L. J. Zhu, J. Zhang,
Prof. G. S. Huang, Dr. J. Wang, Prof. Y. F. Mei
Department of Materials Science
Fudan University
Shanghai 200433, P. R. China
E-mail: yfm@fudan.edu.cn
Prof. G. S. Huang
National Key Laboratory of Fundamental Science of Micro/Nano-Device and System Technology
Chongqing University
Chongqing 400030, P. R. China
Dr. J. Wang
School of Information Science and Engineering
Fudan University
Shanghai 200433, P. R. China

DOI: 10.1002/adom.201500776

2. Results and Discussions

2.1. Fabrication and Characterization

Rolling up of a nanomembrane involves two steps as shown in **Figure 1**a: (i) a sacrificial layer (blue color) and a prestressed functional layer (red) deposited onto a substrate (gray) and (ii) selective removal of the sacrificial layer and release (rolling) of the functional layer. In order to fabricate oxide microtubes with a broad range of diameters, both wet chemical and dry etching methods are adopted in our work. In the wet chemical etching method, a polymer photoresist layer (ARP-3510 from Allresist GmbH) is used and undercut by acetone.[7] In the dry etching method, another polymer layer

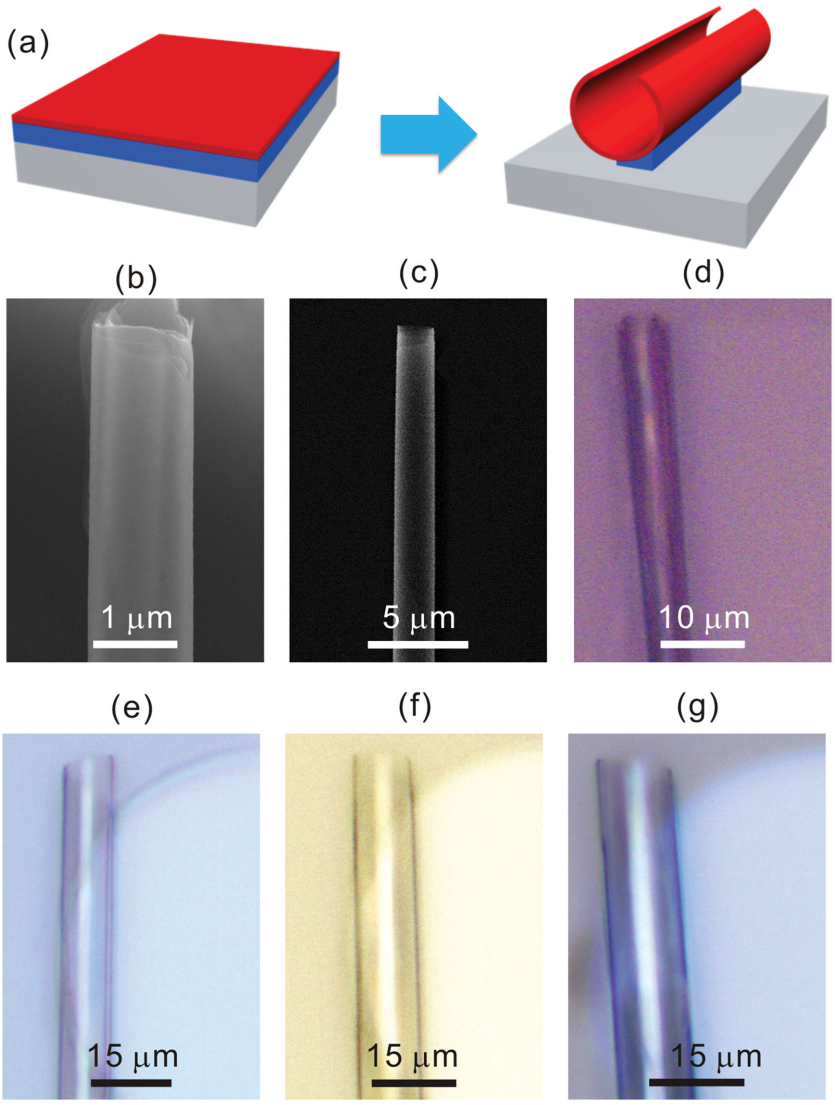

Figure 1. a) Schematic diagram of a rolling-up process with under-etching of a sacrificial layer (blue). b,c) SEM and d–g) optical images of rolled-up oxide microtubes in diverse diameters (D) made out of bilayers: b) SiO_2/TiO_2, D = 1.3 μm; c) SiO/SiO_2, D = 1.7 μm; d) SiO/SiO_2, D = 6.2 μm; e) SiO/SiO_2, D = 9.2 μm; f) SiO/SiO_2, D = 11.6 μm; g) Y_2O_3/ZrO_2, D = 12.7 μm.

(Polymetylmethacrylate, PMMA) is used and removed by the thermal burning.[22] Figure 1b–g shows the images of rolled-up oxide microtubes: (b) SiO_2/TiO_2, (c) SiO/TiO_2, (d) SiO/SiO_2, (e) SiO/SiO_2, (f) SiO/SiO_2, (g) Y_2O_3/ZrO_2, with different diameters (1.1, 1.7, 2.7, 5.8, 9.3, 11.7 μm, respectively). The sequence of layers means the first deposition layer and the second deposition layer, which can enhance the strain gradient for rolling.[7] Figure 1b,c shows scanning electron microscope (SEM) images of rolled-up microtubes with diameters below 5 μm, which are fabricated by the dry etching method (see the Experimental Section). The diameter of microtubes produced by these two methods can be well-tuned by adjusting deposition parameters such as the wall thickness and the deposition rates of the function layers as reported previously.[7,22] The other microtubes with diameters above 5 μm in Figure 1 are obtained by wet-chemical-etching method (see the Experimental Section). It should be mentioned that the microtubes with diameters below 5 μm can also be fabricated by wet chemical etching method when the prestressed layer is very thin and down to several nanometers, which thus could not support the optical resonance. However in our experiments, the rolled-up microtubes with thick walls exhibit the WGM resonance modes as described below (see details in Part 2 of the Supporting Information).

2.2. Resonance Modes

2.2.1. Quality Factors

Figure 2 shows the μ-PL spectra of oxide microtubular microcavities made out of (a) SiO_2/TiO_2, (b) SiO/TiO_2, (c) SiO/TiO_2, (d) SiO/SiO_2, (e) Y_2O_3/ZrO_2, (f) Y_2O_3/ZrO_2, with corresponding diameters (1.1, 1.7, 2.7, 5.8, 9.3, 11.7 μm, respectively) and Q-factors (8, 43, 432, 341, 627, 932, respectively), and the variation trend of the mode peaks can be directly identified with assistant of calculations. With increasing diameters, the spacing of adjacent modes (free spectral range) gets closer. In all these spectra, the observed broad emission band can be assigned to defect-related emission centers (see details in Part 5 of the Supporting Information),[7,23,24,] while the spectra modulation is ascribed to the WGMs in such tubular optical microcavity. Interestingly, a primary resonant peak is accompanied by several subordinate peaks as shown in **Figure 3**c,e. The spectrum in (c) can be ascribed to the 3D confinement[5] and one in (e) is clarified as different polarization modes, i.e., TE (transverse electric, the electric field E parallel to the tube axis) modes.[2] The details can be found in Part 1 of the Supporting Information). Also, the Q-factors of these microtubes are not in a certain discipline mainly due to different wall thicknesses and effective indices.[2] If the effective index constant keeps the same for certain microtubes, when increasing the tube diameter, their quality factors (Q-factor) increase as well due to the wall thickness increases,[2] which can be well explained by the theoretical calculation.

Mie scattering theory is adopted as a calculation method for Q-factors in tubular optical microcavities.[26] We fit the PL spectrum for an outer diameter of 5.8 μm in order to check the consistency between the experimental data and the theoretical simulations (see details in Part 3 of the Supporting Information). Figure 3a shows the calculated resonance spectra of a tubular optical microcavity with diameter of 5.8 μm when changing the wall thickness from 50 to 60 nm. Their Q-factors vary with the wall thickness as well as their resonance wavelengths. Q-factors are extracted from the spectra in Figure 3a

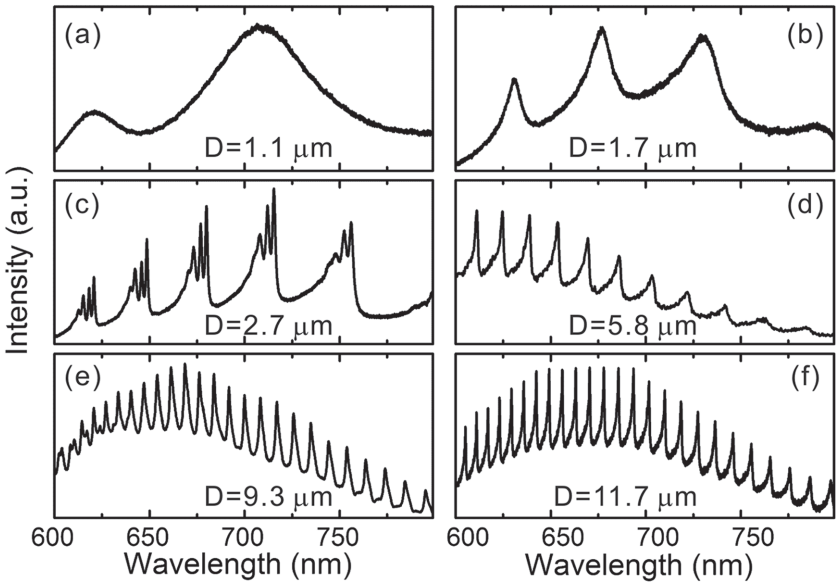

Figure 2. PL spectra from microtubes with different diameters made out of a) SiO_2/TiO_2, D = 1.1 μm; b) SiO/TiO_2, D = 1.7 μm; c) SiO/TiO_2, D = 2.7 μm; d) SiO/SiO_2, D = 5.8 μm; e) Y_2O_3/ZrO_2, D = 9.3 μm; f) Y_2O_3/ZrO_2, D = 11.7 μm, which are corresponding to panels (b)–(g) in Figure 1.

and plotted in Figure 3b. It is obvious that Q-factors decrease rapidly with increased wavelengths since the tube wall thicknesses relatively decrease if the resonance wavelengths increase. As the tube wall is too thin to confine the light with attenuated total reflection, a small increment of the tube wall thickness (equivalent to the wavelength decrement) causes a drastic enhancement of Q-factors. These calculated results on relationship between Q-factors and wall thickness of tubular microcavities consistent with the experimentally results of our previous report.[27]

2.2.2. Mode Spacing

The WGM resonance condition in tubular microcavities with tunable diameters is $2\pi R n_{\text{eff}} = m\lambda$, where R is the average radius of the microtube, λ is the resonant wavelength, n_{eff} is the effective refractive index of the wall and m is the azimuthal number. Thus, the mode spacing energy (or free spectral range) can be described as[26]

$$\Delta E = \frac{hc}{\pi} \frac{1}{D n_{\text{eff}}} \tag{1}$$

Based on the planar waveguide model, we can calculate the effective refractive index as the function of the thickness/diameter of six microtubes from their geometries (radius/thickness) and bulk refractive indices. The propagation constants β in a flat waveguide satisfy[27]

$$2t - \left(1 - t^2\right)\tan\left(q_f \Delta\right) = 0 \tag{2}$$

where $t = q_b/q_f$ for TE modes, $q_b^2 = \beta^2 - \varepsilon_b k_0^2$, $q_f^2 = \varepsilon_f k_0^2 - \beta^2$, $k_0 = 2\pi/\lambda$ (λ is the wavelength in vacuum, ε_b is the dielectric constant of background, and the average dielectric constant ε_f of the film equal to n_{eff}^2). To give a clear explanation on the relationship between the tube geometries and n_{eff}, we fit the curves in **Figure 4**a based on the experimental data in Figure 2a–f and thus get the specific n_{eff} of each microtube. As shown in Figure 4a, for a certain diameter, the n_{eff} increases with the wall thickness. When the wall thickness is thick enough, its impact on n_{eff} gets weak, and thus the curve changes gently. Therefore the n_{eff} is changing slightly for all tubes described in Figure 2a–f as shown in Figure 4a, from which we can calculate the mode spacing to fit the experimental data (black spheres in Figure 4).

Equation (1) indicates that the mode spacing ΔE is inversely proportional to $D \cdot n_{\text{eff}}$ of the tubular oxide microcavities. In Figure 4b, the six experimental points from Figure 2a–f (black sphere) demonstrate that ΔE decreases with the $D \cdot n_{\text{eff}}$ increasing. The experimental data (black spheres) well agrees with equation (1) (gray line) as shown in Figure 4 b. Since the n_{eff} varies little, the mode space ΔE is mainly determined by the tube diameters. Thus, the larger diameters introduce the smaller spacing of adjacent mode peaks. One can see that with increasing D, more optical modes can be detected from the same spectra range due to the decrease of ΔE. If the microtube thickness is thick enough, the n_{eff} becomes closer to the refractive index of the bulk materials. The resonance wavelengths should be only determined by the diameter, which then is similar to other WGM microcavities.[28,29]

2.3. Resonance Coupling

2.3.1. Photoluminescence

In order to demonstrate the resonance coupling into the tube wall, R6G molecules were introduced onto the wall of the rolled-up microtube as shown in **Figure 5**a. To avoid the damage from treatments, rolled-up oxide microtube was reinforced with 30 nm thick Al_2O_3 coating by atomic layer deposition (ALD) method. Then, the poly(diallyldimethylammonium chloride) (PDDA)/inpoly(acrylic acid) (PAA) bilayer incorporated with Rhodamine 6G molecules is coated on the wall of the self-rolled microtube by layer by layer (LBL) coating.[30] The details are described in the Experimental Section. The inset in Figure 5b schematically depicts the multilayer structure of the tube wall after Al_2O_3 coating and LBL coating. The optical properties of these oxide tubular microcavities were characterized by μ-PL spectroscopy at room temperature with an excitation line at 532 nm. The spectra of both as-fabricated and R6G-incorporated tubular microcavities are shown in Figure 5b. The as-fabricated one is noted as Y_2O_3/ZrO_2 and the R6G-incorporated one is noted as PAA/ Y_2O_3/ZrO_2. All the modes are marked by their azimuthal mode number m with careful calculation and assignment. PL Measurements on the original

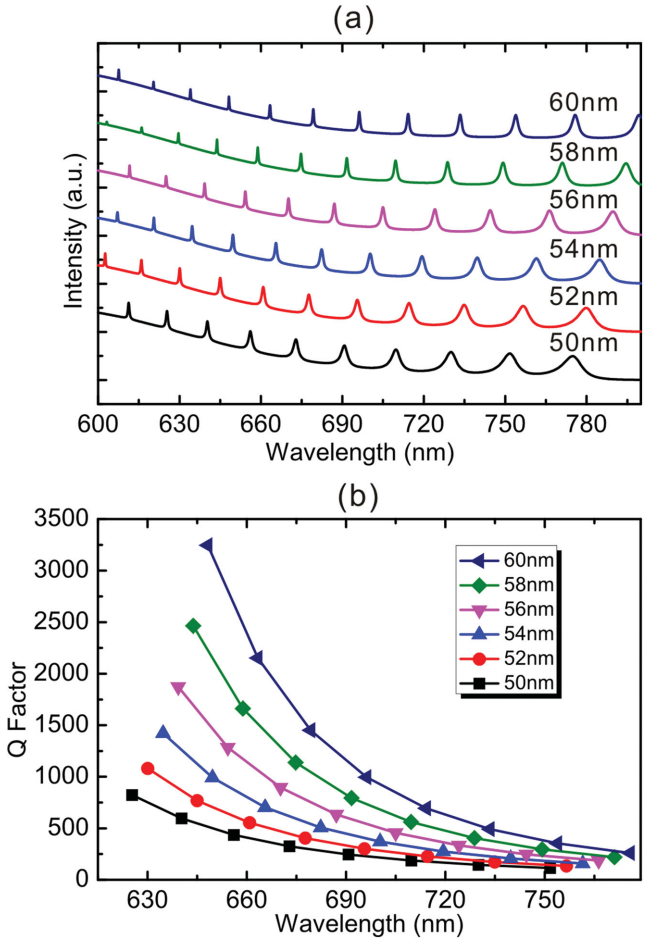

Figure 3. a) Theoretical PL spectra of microtubes with different wall thickness from 50 to 60 nm. The outer diameter is fixed at 5.8 μm and refractive index is 2. b) Theoretical *Q*-factors extracted from a).

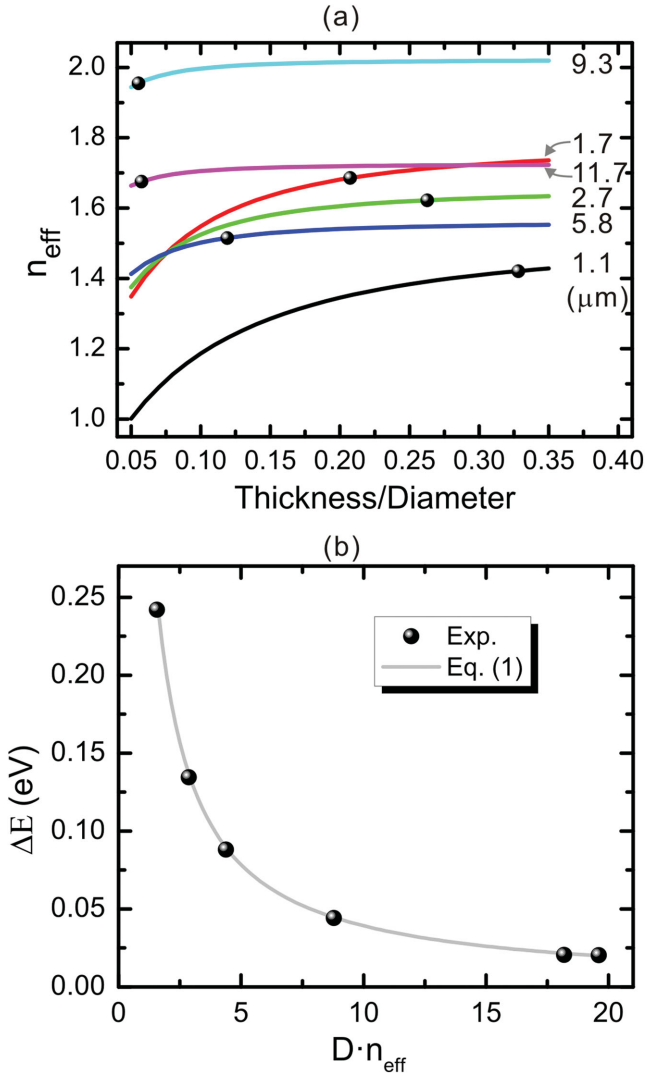

Figure 4. a) The effective refractive index n_{eff} as a function of the thickness/diameter. The black spheres present the data from the tubular oxide microcavities with different diameter in Figures 1 and 2. The solid lines are the fitting curves based on the experimental data points. b) The mode spacing (free spectral range) ΔE of each PL spectrum as a function of $D \cdot n_{eff}$, where D is taken from the experimental data and n_{eff} is from panel (a). The black spheres present the experimental data points and the gray line is from Equation (1).

Y_2O_3/ZrO_2 microtube reveal the defect-related emission centers of the tube itself at ≈670 nm and the typical mode sequences of the specific Y_2O_3/ZrO_2 microtube are as observed in previous experiments.[31] After LBL coating, a broad emission peak with a blue shift below 600 nm is found and close to the intrinsic emission peak of the dye emitter R6G at around 550 nm since the excitation line at 532 nm is used. The superposition and the shift of optical modes on the broad emission peaks of the coated microtube clearly demonstrate the effective coupling of the dye emitters (see the details in Part 6 of the Supporting Information). Interestingly, the *Q*-factors can be even enhanced under the coupling condition due to the increasing wall thickness after LBL coating. The *Q*-factor of tubular microcavity ($m = 84$, $\lambda = 665$ nm) before and after LBL coating is 306 and 631, respectively. Therefore, we may incorporate interesting luminescent materials into the tubular microcavity via the coupling in the nonevanescent regimes.

2.3.2. Raman Scattering

Besides the incorporation of dye in the tube wall, the molecular absorption on the surface can enable the resonance working in the nonevanescent regimes as well, which can serve for cavity enhanced Raman scattering if the WGM resonances occur at the range of the incident excitation wavelength and the Raman shifted Stokes wavelengths.[32–34] We demonstrate rolled-up tubular SiO/TiO_2 microtubes as optical microcavity for enhanced Raman scattering. The rolled-up tubular SiO/TiO_2 microtubes with diameter of 1.7 μm are coated with 20 nm Al_2O_3, and afterward, R6G solution was dropped onto the ALD-coated SiO/TiO_2 tubular microcavity as well as the flat SiO/TiO_2 bilayer film. The Raman measurement was conducted after the samples are dried in the air by using an excitation wavelength of 514 nm. The dye molecules can be well absorbed into the tube wall since the deposited films are always rough and even with tiny holes. **Figure 6**a shows the corresponding

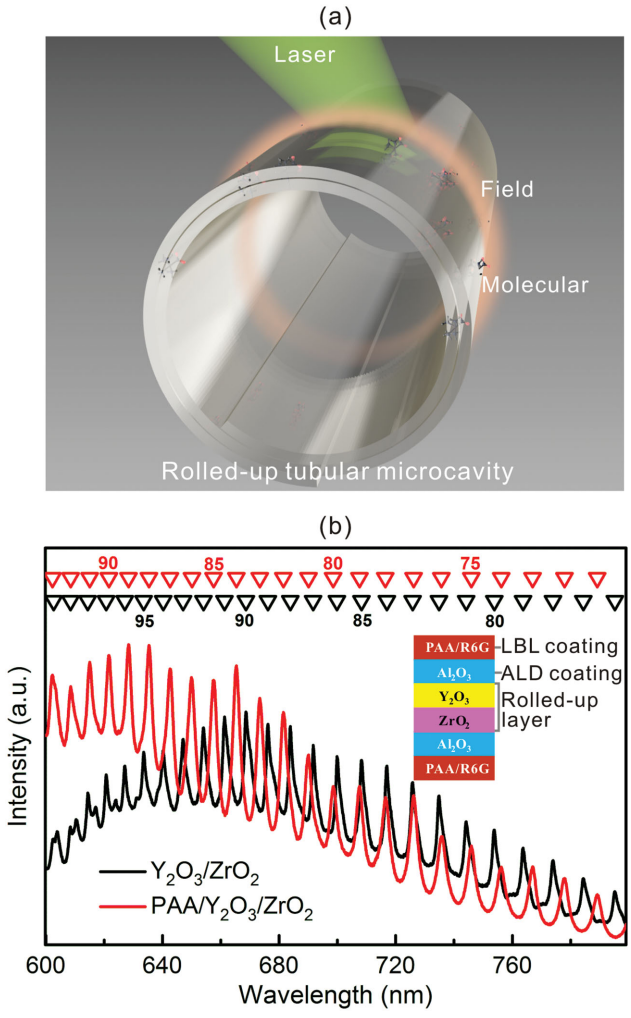

Figure 5. a) Sketch of a rolled-up tubular microcavity incorporated with dye emitters, which can be excited by green laser (532 nm) for on-resonance coupling. b) The PL spectrum collected from the Y_2O_3/ZrO_2 tubular microcavity with 30 nm Al_2O_3 ALD coating under a laser excitation wavelength 532 nm. The inset is a schematic diagram of the cross-sectional view of the microtube wall after Al_2O_3 coating and LBL coating with the dye. The modes are marked by their azimuthal mode number *m*. The black line and the red line respectively show the PL spectrum of the Y_2O_3/ZrO_2 microtube without and with LBL-coated dye emitters.

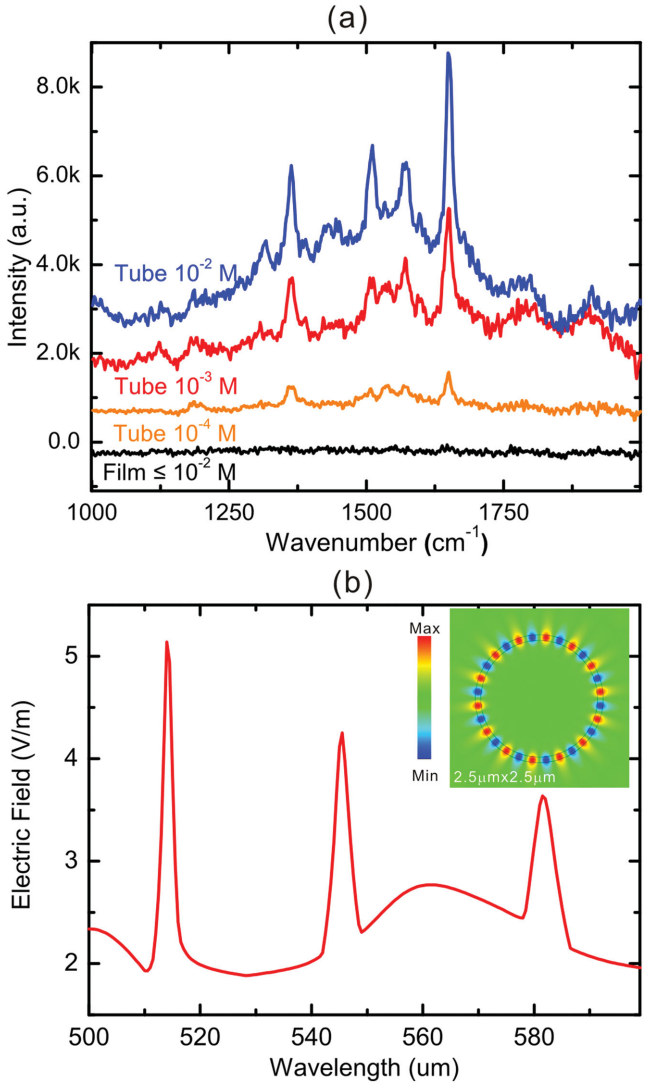

Figure 6. a) Raman spectra collected from tubular microcavity rolled from a prestressed SiO/TiO_2 bilayer nanomembrane with ≈20 nm Al_2O_3 ALD-coating under the excitation wavelength of 514 nm. The black line shows the Raman spectrum of the original SiO/TiO_2 nanomembrane with R6G solution (10^{-2} to 10^{-4} mol L^{-1}, M refers to mol L^{-1}) and the other color lines depict the SiO/TiO_2 microtube with R6G solution of different concentration. b) The electric filed of the microtube as a function of wavelengths. The inset shows calculated on-resonance field profiles (azimuthal mode number, $m = 15$) with a 514 nm excitation line in tubular microcavity with 1.7 μm diameter.

Raman spectra with different R6G solution concentrations. The black line indicates the Raman spectrum of the SiO/TiO_2 bilayer film with 10^{-2} mol L^{-1} R6G solution. Repeated experiments revealed that the Raman scattering peaks could not be detected on the bilayer film when the solution concentration is below 10^{-2} mol L^{-1} and the lines are almost the same with the black one. However, significantly enhanced Raman spectra are observed from the tubular structure in 10^{-2} mol L^{-1} R6G solution and below. Figure 6a demonstrates the correlation between the effect of enhanced Raman scattering and the concentration of the R6G solution, which is a positive correlation since the higher concentration, the higher enhancement and the enhancement factor can approach the order of more than 10^2.

WGMs in microcavities can lead to a dramatically enhancement of the local electromagnetic field around the thin walls of microtubes. Mie scattering method was applied to calculate the electric field enhancement of the WGMs in the rolled-up microtube. The inset of Figure 6b depicts the average electric field intensity at the excitation laser wavelength in a tubular optical microcavity with the diameter of 1.7 μm, where the azimuthal mode number of optical resonance is 15 under TM modes (TM: transverse magnetic, the electric field E perpendicular to the tube axis). The electric filed is calculated by Mie scattering theory, which shows that resonance modes are confined in the tube wall.[26] Taking the microtube with the diameter of 1.7 μm

and an average refractive index of 1.95, the calculated maximum field strength in the tube is 4.55 V m^{-1}, thus the enhancement factor of Raman intensities approach the order of 10^2 when it is illuminated by a plane wave of 1 V m^{-1} at 514 nm, which is shown in Figure 6b. The experimental *Q*-factors in our microtubes are always smaller than the calculated values. It means the resonance peak at 514 nm can be slightly broad and thus cover the incident excitation wavelength and/or the Raman shifted Stokes wavelength.[33] Different from the normal WGM sensing based on resonance shift or FSR change,[35] our results indicate that oxide tubular microcavities can be used to enhance Raman signal detection with the coupling of the dye molecules into the nonevanescent regimes, which may suggest interesting coupling with optical microcavities for applications in detection and lasing.[15,16]

3. Conclusion

Self-rolling of oxide nanomembranes into tubular structures allows a cheap and convenient way to fabricate transparent tubular optical microcavities with a broad range of diameters, which therefore offer flexible tuning of the resonance modes. The efficient coupling of dye emitters at the nonevanescent-regimes of optical resonance in rolled-up oxide tubular microcavities are proved by photoluminescence measurement and Raman scattering. The latter can be also enhanced more than 10^2 times due to the on-resonance of the excitation wavelength and/or the Raman shifted Stokes wavelengths. Our approach suggests that rolled-up tubular optical microcavity can be an interesting optical platform to explore the coupling between resonance modes and matters, such as 2D materials[36] or high fluorescence materials.[37]

4. Experimental Section

Microtube Fabrication: Wet chemical[7] and dry etching methods[22] were used for the fabrication of rolled-up microtubes with various diameters. For wet chemical etching method, the formation process started with spin-coating of a uniform ≈2 μm thick ARP-3510 photoresist (Allresist GmbH) layer on Si wafer, which was defined into circles with various sizes by photolithography and served as a sacrificial layer in the following rolling process. The strained oxide bilayer nanomembranes were deposited by e-beam evaporation with glancing angle (the angle is 60°), which can guarantee the tubes attached on substrates.[7] Acetone was applied to selectively remove the photoresist layer and release (roll up) the functional oxide bilayer. The intrinsic stress gradient enabled the bilayered nanomembrane self-rolled up into a tubular microcavity. The rolled-up oxide microtubes were then dried in the critical point dryer (Leica CPD 030) by using liquid CO_2 as an inter-media to avoid the collapse of the tubular structures.

By contrast, the dry-releasing method is supposed to roll up nanomembranes into tubular microcavities by burning of a sacrificial layer. Polymetylmethacrylate (PMMA, 5 wt% in acetone) was firstly spin-coated on silicon substrate as a sacrificial layer, and an oxide bilayer nanomembrane were deposited subsequently by electron beam evaporation onto the PMMA layer. Rapid thermal annealing (ULVAC, ACS-4000-C4) was conducted afterward to release the prestrained oxide nanomembrane. The annealing temperature was set at 600 °C and the annealing time was 40 s. Therefore, the oxide nanomembrane released from the sacrificial layer due to the burning-up of PMMA during annealing and rolled up into a tubular structure with a diameter of below 2 μm. Consequently, as-prepared rolled-up microtubes with tunable diameters can be achieved by controlling the nanomembrane thickness and the deposition parameters.

Layer-by-Layer Coating: The molecule R6G was chosen as a dye emitter to be introduced into the wall of the self-rolled tubular microcavity. These R6G molecules dispersed into poly-acrylic-acid (PAA) polymer were coated onto the microtube wall by layer-by-layer (LBL) coating.[30] In order to prevent the Y_2O_3/ZrO_2 microtube from sticking on substrates and collapse by themselves due to the liquids inside the tubes while LBL coating, 30 nm Al_2O_3 coating were firstly deposited by ALD to increase the wall thickness and be able to sustain the repeated liquid washing of the LBL coating solution. LBL coating was based on developing hierarchical micro/nanostructured surfaces by the alternating deposition of the polycation at high pH and the polyanion at low pH, thus provided a simple and versatile tool for constructing ultrathin films with functionalities. The microtube sample was immersed into poly-diallyldimethylammonium chloride (PDDA, 200 000, 20 wt%, Aldrich) for 15 min pretreatment to get a polycation layer and then washed it in deionized water (DI water) for four times (1 min at each turn). Then, the microtube sample was immersed into PAA (450 000, 1 mg/ml, 10 ml) mixed with 1 mg R6G for 15 min and washed in DI water for four times (1 min at each turn). The process was only done once, which was enough for the dye incorporation. The LBL layer was then thermally cross-linked by annealing process at 130 °C for 2.5 h.

Supporting Information

Supporting Information is available from the Wiley Online Library or from the author.

Acknowledgements

This work was supported by the Natural Science Foundation of China (Grant Nos. 51322201, 51475093, and 51302039), Specialized Research Fund for the Doctoral Program of Higher Education (Grant No. 20120071110025), Science and Technology Commission of Shanghai Municipality (Grant No. 14JC1400200), and Visiting Scholar Foundation of National Key Laboratory of Fundamental Science of Micro/Nano-Devices and System Technology in Chongqing University (Grant No. 2014MS03). Part of the experimental work had been carried out in Fudan Nanofabrication Laboratory.

Received: December 24, 2015
Revised: January 25, 2016
Published online: March 7, 2016

[1] X. Li, *Adv. Opt. Photonics* **2011**, *3*, 366.
[2] J. Wang, T. Zhan, G. Huang, P. K. Chu, Y. F. Mei, *Laser Photonics Rev.* **2014**, *8*, 521.
[3] S. Yang, Y. Wang, H. Sun, *Adv. Optical Mater.* **2015**, *3*, 1136.
[4] X. Jiang, C. Zou, L. Wang, Q. Gong, Y. Xiao, *Laser Photonics Rev.* **2015**, *1*, 22.
[5] T. Kipp, H. Welsch, C. Strelow, C. Heyn, D. Heitmann, *Phys. Rev. Lett.* **2006**, *96*, 077403.
[6] F. Li, Z. Mi, S. Vicknesh, *Opt. Lett.* **2009**, *34*, 2915.
[7] Y. F. Mei, G. Huang, A. A. Solovev, E. B. Ureña, I. Mönch, F. Ding, T. Reindl, R. K. Y. Fu, P. K. Chu, O. G. Schmidt, *Adv. Mater.* **2008**, *20*, 4085.
[8] I. M. White, H. Oveys, X. Fan, *Opt. Lett.* **2006**, *31*, 1319.
[9] X. Fan, I. M. White, S. I. Shopova, H. Zhu, J. D. Suter, Y. Sun, *Anal. Chim. Acta* **2008**, *620*, 8.

[10] G. S. Huang, V. A. Bolaños Quiñones, F. Ding, S. Kiravittaya, Y. F. Mei, O. G. Schmidt, *ACS Nano* **2010**, *4*, 3123.
[11] Y. P. Rakovich, S. Balakrishnan, J. F. Donegan, T. S. Perova, R. A. Moore, Y. K. Gun'Ko, *Adv. Funct. Mater.* **2007**, *17*, 1106.
[12] K. J. Vahala, *Nature* **2003**, *424*, 839.
[13] Y. Yamamoto, R. E. Slusher, *Phys. Today* **1993**, *46*, 66.
[14] K. Dietrich, C. Strelow, C. Schliehe, C. Heyn, A. Stemmann, S. Schwaiger, S. Mendach, A. Mews, H. Weller, D. Heitmann, T. Kipp, *Nano Lett.* **2010**, *10*, 627.
[15] X. Fan, I. M. White, *Nat. Photon.* **2011**, *5*, 591.
[16] D. Psaltis, S. R. Quake, C. Yang, *Nature* **2006**, *442*, 381.
[17] T. Ling, L. J. Guo, *J. Opt. Soc. Am. B* **2009**, *26*, 471.
[18] T. Ling, L. J. Guo, *Opt. Express* **2007**, *15*, 17424.
[19] B. B. Li, W. R. Clements, X. C. Yu, K. Shi, Q. Gong, Y. F. Xiao, *Proc. Natl. Acad. Sci. USA* **2014**, *111*, 14657.
[20] M. Larsson, K. N. Dinyari, H. Wang, *Nano Lett.* **2009**, *9*, 1447.
[21] L. Ma, S. Li, V. A. B. Quiñones, L. Yang, W. Xi, M. Jorgensen, S. Baunack, Y. F. Mei, S. Kiravittaya, O. G. Schmidt, *Adv. Mater.* **2013**, *25*, 2357.
[22] J. Li, J. Zhang, W. Gao, G. Huang, Z. Di, R. Liu, J. Wang, Y. F. Mei, *Adv. Mater.* **2013**, *25*, 3715.
[23] L. X. Yi, J. Heitmann, R. Scholz, M. Zacharias, *Appl. Phys. Lett.* **2002**, *81*, 4248.
[24] A. Madani, S. Boettner, M. Jorgensen, O. G. Schmidt, *Opt. Lett.* **2014**, *39*, 189.
[25] F. S. De Vicente, A. C. De Castro, M. F. De Souza, M. Siu Li, *Thin Solid Films* **2002**, *418*, 222.
[26] T. Zhan, C. Xu, F. Zhao, Z. Xiong, X. Hu, G. Huang, Y. F. Mei, J. Zi, *Appl. Phys. Lett.* **2011**, *99*, 211104.
[27] V. A. Bolaños Quiñones, G. Huang, J. D. Plumhof, S. Kiravittaya, A. Rastelli, Y. F. Mei, O. G. Schmidt, *Opt. Lett.* **2009**, *34*, 2345.
[28] F. Vollmer, S. Arnold, *Nat. Methods* **2008**, *5*, 591.
[29] C. H. Dong, L. He, Y. F. Xiao, V. R. Gaddam, S. K. Ozdemir, Z. F. Han, G. C. Guo, L. Yang, *Appl. Phys. Lett.* **2009**, *94*, 231119.
[30] K. Ariga, J. P. Hill, Q. Ji, *Phys. Chem. Chem. Phys.* **2007**, *9*, 2319.
[31] J. Wang, T. Zhan, G. Huang, X. Cui, X. Hu, Y. F. Mei, *Opt. Express* **2012**, *20*, 18555.
[32] J. B. Snow, S. X. Qian, R. K. Chang, *Opt. Lett.* **1985**, *10*, 37.
[33] L. K. Ausman, G. C. Schatz, *J. Chem. Phys.* **2008**, *129*, 054704.
[34] R. Liu, W. Jin, X. Yu, Y. Liu, Y. Xiao, *Phys. Rev. A* **2015**, *91*, 043836.
[35] V. Ta, R. Chen, L. Ma, Y. Ying, H. Sun, *Laser Photonics Rev.* **2013**, *7*, 133.
[36] O. Salehzadeh, M. Djavid, N. H. Tran, I. Shih, Z. Mi, *Nano Lett.* **2015**, *15*, 5302.
[37] H. Zhu, Y. Fu, F. Meng, X. Wu, Z. Gong, Q. Ding, M. V. Gustafsson, M. T. Trinh, S. Jin, X. Zhu, *Nat. Mater.* **2015**, *14*, 636.